Efficient jacobian matrix for the MCSEM 2.5D

Camila N. Castro* (Federal University of Pará, Brazil) e Marcos Welby C. Silva (Federal University of Pará, Brazil)

Abstract

In the last 20 years the marine controlled-source electromagnetic method has taken its place in the hydrocarbon industry and it has been used continuously as an auxiliary tool in the exploration workflow. As consequence, the modeling and inversion of electromagnetic data have been improved constantly. In this work, we develop the mathematical formulation of the self-adjoint method applied to MCSEM for the most efficient calculation of the jacobian matrix. The computational implementation and validation were done in Fortran using the bi-dimensional finite element method in a model with twelve inversion parameters.

Introduction

In the last two decades, there is a growing interest in the exploration of hydrocarbons in the marine environment. One of the methods extensively used is the marine Controlled Source Electromagnetics (MCSEM) which has a good potential for the detection and mapping of offshore resistive bodies (e.g. Buonora et al., 2014). Initially, the MCSEM was developed for applications in the study of the lithosphere and with the electronic advancement of equipment, this method was improved and applied in the exploration of hydrocarbons.

In the modeling of MCSEM, the most traditional numerical techniques are used, such as Integral Equation (IE), (Ueda and Zhdanov (2005), Gribenko and Zhdanov (2007) and Bakr and Mannseth (2009)), Finite Elements (FE) (Silva (2012),Nalepa et al. (2016) and Bakr and Pardo (2014)) and Finite Difference (FD) (Frenkel and Davydycheva (2009), Maaø (2007) and Zach et al. (2012)).

While advances in numerical modeling were achieved, progress was also made in solving the inverse problem using different inversion techniques. We can cite the non-linear Gauss-Newton numerical method (Tarantola and Valette (1982), Peng and Hu (2015)), BFGS method (Li et al. (2013), Nguyen et al. (2016) and Li and Li (2017)) and OCCAM method (Constable et al. (1987), Ramananjaona et al. (2011) and Moghadas et al. (2015)).

The inverse geophysical problem is directly dependent on an accurate modeling algorithm, called the direct problem. The methodologies used in inversion consist, in different ways, of solving a linear system that represents the geophysical problem. In almost all of them it is necessary to use the jacobian matrix associated with the data from the marine controlled source method.

In this work, the calculation of the jacobian matrix was performed using the self-adjoint method associated with MCSEM. However, this methodology has already been used with different applications: in Gomes and Silva (2021) it was applied to the Magnetoteluric method, in Taillandier et al. (2009) and Shragge et al. (2013) to seismic tomography.

This work aims at an application of the self-adjoint method, which consists of the use of the fields $\mathbf{H}_y^s$ and $\mathbf{E}_y^s$ in the construction of the jacobian for the MCSEM method. For validation, a comparison was made between the self-adjoint method and the finite difference method using perturbations of the parameters (Brute Force). The results obtained prove the efficiency of the self-adjoint method in the calculation of the jacobian matrix for the MCSEM method.

Methodology

Geophysical inversion is the mathematical computational process that seeks to estimate the physical parameters of a given region in which geophysical observations were acquired. In MCSEM, these physical parameters are the distribution of electrical resistivity (or conductivity) in the subsurface. Some of the various geophysical data inversion techniques use a methodology that relates the observed data to its derivatives. Thus, the first important step in this process is the calculation of the MCSEM observations, which are amplitude and phase of the electric field $\mathbf{E}_x$ (inline component). The second step is to find the derivatives of this data in relation to the physical parameter. In the following paragraphs, we will show the mathematical development necessary for the estimation of these quantities.

Calculation of the observations' derivatives in relation to the parameters

We will solve the direct problem using the finite element method, in which we have a linear system that is represented by the equation below:

$$\mathbf{S}\mathbf{x} = \mathbf{h}, \tag{1}$$

where $\mathbf{S}$ is the global matrix associated with the properties of the environment , $\mathbf{h}$ is the source vector of the problem represented by the horizontal electric dipole and $\mathbf{x}$ is the solution vector of the system that consists of the fields $\mathbf{E}_y$ and $\mathbf{H}_y$ associated with MCSEM. It is precisely from these components that we will obtain the amplitude and phase of the field $\mathbf{E}_x$. The mathematical development and implementation of the finite element method for this problem and its solution can be found at Silva (2012). In that work, the solution was obtained by separating

the electromagnetic fields in their primary and secondary components, the formulation of finite elements is done using the fields $\mathbf{E}_y^s$ and $\mathbf{H}_y^s$.

The observations of MCSEM are given in terms of the electric field component $\mathbf{E}_x$ (inline). It can be written in complex exponential form:

$$\mathbf{E}_x = |\mathbf{E}_x| e^{i\phi}, \tag{2}$$

Differentiating in relation to resistivity we obtain:

$$\frac{1}{\mathbf{E}_x}\frac{\partial \mathbf{E}_x}{\partial \rho_i} = \frac{1}{|\mathbf{E}_x|}\frac{\partial |\mathbf{E}_x|}{\partial \rho_i} + i\frac{\partial \phi}{\partial \rho_i}. \tag{3}$$

According to Rijo et al. (1977), using the natural log of resistivity makes the process faster, more efficient and more stable. Mainly due to numerical convergence, inversions are made in relation to the resistivity log. In addition, parameterization has the beneficial effect of excluding negative resistivities from the considerations as possible solutions. The natural log is also used in the absolute value of the $\mathbf{E}_x$ field, since MCSEM has wide variations in the $\mathbf{E}_x$, ranging from approximately 10^{-15} a 10^{-8} V/m which can generate extreme variation in the observed data.

Thus, separating the complex function (3) into its real and imaginary parts and applying the natural log, we obtain:

$$\frac{\partial \ln |\mathbf{E}_x|}{\partial \ln \rho_i} = -\sigma_i Re\left\{\frac{1}{\mathbf{E}_x}\frac{\partial \mathbf{E}_x^s}{\partial \sigma_i}\right\} \tag{4}$$

$$\frac{\partial \phi}{\partial \ln \rho_i} = -\sigma_i Im\left\{\frac{1}{\mathbf{E}_x}\frac{\partial \mathbf{E}_x^s}{\partial \sigma_i}\right\} \tag{5}$$

The terms $\frac{\partial \ln |\mathbf{E}_x|}{\partial \ln \rho_i}$ e $\frac{\partial \phi}{\partial \ln \rho_i}$ of the equations (4) and (5) will compose the lines of the jacobian matrix of the i-th column related to the resistivity parameter.

The code used to develop this work uses the conductivity of the medium instead of the resistivity and for that reason the derivative of the observations in relation to the parameters will be given in terms of the derivative of the field $\mathbf{E}_x$ in relation to the conductivity σ_i.

Therefore, in the domain of the transformed *y*, we will calculate the derivative of $\mathbf{E}_x^s$ in relation to σ_i.

According to the work of Silva (2012), the field $\mathbf{E}_x^s$ can be defined using the equation (6) with $\hat{z}$ as impedance $\hat{z} = i\omega\mu_0$, $\hat{y}$ admittance, defined by $\hat{y} = \sigma + i\omega\varepsilon$ and $u = \sqrt{k_y^2 + i\omega\mu_0\sigma_i}$, k_y being the space wave number in the Fourier transform domain:

$$\hat{\mathbf{E}}_x^s = -\frac{ik_y}{u^2}\frac{\partial \hat{\mathbf{E}}_y^s}{\partial x} - \frac{\hat{z}}{u^2}\frac{\partial \hat{\mathbf{H}}_y^s}{\partial z} - \frac{\hat{z}\Delta\sigma_i}{u^2}\hat{\mathbf{E}}_x^p. \tag{6}$$

Using the definition of (Silva, 2012) for the derivatives of the fields $\mathbf{E}_y^s$ and $\mathbf{H}_y^s$ in relation to the x and z coordinates represented in the equations below:

$$\frac{\partial \hat{\mathbf{E}}_y^s}{\partial x} = -\hat{z}\hat{\mathbf{H}}_z^s + ik_y\hat{\mathbf{E}}_x^s, \tag{7}$$

$$\frac{\partial \hat{\mathbf{H}}_y^s}{\partial z} = -\hat{y}\hat{\mathbf{E}}_x^s + ik_y\hat{\mathbf{H}}_z^s - \Delta\sigma_i\hat{\mathbf{E}}_x^p, \tag{8}$$

the calculation of the derivative $\frac{\partial \mathbf{E}_x^s}{\partial \sigma_i}$ is defined by the equation below:

$$\frac{\partial \hat{\mathbf{E}}_x^s}{\partial \sigma_i} = -\frac{ik_y}{u^2}\frac{\partial^2 \hat{\mathbf{E}}_y^s}{\partial \sigma_i \partial x} - \frac{\hat{z}}{u^2}\frac{\partial^2 \hat{\mathbf{H}}_y^s}{\partial \sigma_i \partial z} - \frac{\hat{z}}{u^2}\hat{\mathbf{E}}_x^t \tag{9}$$

Formulation of the Adjoint-State Method

The calculation of the derivatives $\frac{\partial \hat{\mathbf{E}}_y^s}{\partial \sigma_i}$ and $\frac{\partial \hat{\mathbf{H}}_y^s}{\partial \sigma_i}$ will be given from the derivation of the equation (1) in relation to the parameter σ_i to obtain:

$$\frac{\partial \mathbf{x}}{\partial \sigma_i} = \mathbf{S}^{-1}\left(\frac{\partial \mathbf{h}}{\partial \sigma_i} - \frac{\partial \mathbf{S}}{\partial \sigma_i}\mathbf{x}\right). \tag{10}$$

in the equation (10), we can see that there is a new linear system in a format similar to the equation (1) with the new source represented by the term in parentheses and the same global matrix $\mathbf{S}$ that relates parameter of the geological environment with the finite element mesh. The solution contains the derivatives we want to calculate, in which the vector $\frac{\partial \mathbf{x}}{\partial \sigma_i}$ has the derivatives $\frac{\partial \hat{\mathbf{E}}_y^s}{\partial \sigma_i}$ e $\frac{\partial \hat{\mathbf{H}}_y^s}{\partial \sigma_i}$ organized from interspersed way for each mesh node.

Although the two systems have different solutions, they share the same matrix $\mathbf{S}$ therefore, when solving the direct problem, we use the already factored matrix from the system of the equation (1) to obtain the two solutions. This implies a reduction in the processing time of the second system of the equation (10) and became the calculation of the derivatives quite efficient.

For the purpose of solving the equation (10), we will calculate $\frac{\partial \mathbf{h}}{\partial \sigma_i}$ and $\frac{\partial \mathbf{S}}{\partial \sigma_i}$ respectively. It is important to note that the matrix $\mathbf{S}$ is composed of 3 submatrices $\mathbf{K}$ and to derive $\mathbf{S}$ implies to derive each of the submatrices, the same happen for the source vector $\mathbf{h}$ which is constituted of two subvectors $\mathbf{f}$. Following the finite element methodology found in Silva (2012), this is equivalent to calculating the derivatives of $\mathbf{K}_{tm}$, $\mathbf{K}_{te}$, $\mathbf{K}_{ac}$, $\mathbf{f}_{tm}$ and $\mathbf{f}_{te}$ and then assemble the vectors $\frac{\partial \mathbf{S}}{\partial \sigma_i}$ and $\frac{\partial \mathbf{h}}{\partial \sigma_i}\mathbf{x}$ where $\mathbf{x}$ is the system solution for the equation (1) containing $\hat{\mathbf{E}}_y^s$ e $\hat{\mathbf{H}}_y^s$.

We will start calculating the derivatives of the matrices $\mathbf{K}$ for the coupled modes TM and TE, which can be described by the equations (11), (12) and (13). In that equations, A is the area of each element and $\mathbf{a}_i$, $\mathbf{b}_i$, $\mathbf{c}_i$ are constants associated with the geometry of the elements of the mesh used.

$$\mathbf{K}_{tm} = \frac{\hat{z}}{4Au^2}\left(b_i b_j + c_i c_j\right) + \frac{A\hat{z}}{12}\left(\delta_{ij} + 1\right), \tag{11}$$

$$\mathbf{K}_{te} = \frac{\sigma_i}{4Au^2}\left(b_i b_j + c_i c_j\right) + \frac{A\sigma_i}{12}\left(\delta_{ij} + 1\right), \tag{12}$$

$$\mathbf{K}_{ac} = \frac{ik_y}{4Au^2}\left(b_i c_j - c_i b_j\right). \tag{13}$$

As a result of the derivation of the equations (11), (12), (13), we find the new submatrices:

$$\frac{\partial \mathbf{K}_{tm}}{\partial \sigma_i} = \frac{\omega^2\mu_0^2}{4Au^2}\left(b_i b_j + c_i c_j\right), \tag{14}$$

$$\frac{\partial \mathbf{K}_{te}}{\partial \sigma_i} = \frac{\left(b_i b_j + c_i c_j\right)}{4Au^2}\left(1 - i\omega\mu_0\sigma_i\right) + \frac{A}{12}\left(\delta_{ij} + 1\right), \tag{15}$$

$$\frac{\partial \mathbf{K}_{ac}}{\partial \sigma_i} = \frac{\omega \mu_0 k_y}{4Au^2}\left(b_i c_j - c_i b_j\right). \tag{16}$$

Likewise, the source vector for the TM and TE mode can be described by the equations below:

$$\mathbf{F}_{tm} = -\frac{\hat{z}\Delta\hat{y}}{6u^2} c_i \sum \mathbf{E}_x^p + \frac{\hat{z}\Delta\hat{y}}{6u^2} b_i \sum \mathbf{E}_z^p, \tag{17}$$

$$\mathbf{F}_{te} = -\frac{ik_y \Delta\sigma_i}{6u^2} b_i \sum \mathbf{E}_x^p - \frac{ik_y \Delta\sigma_i}{6u^2} c_i \sum \mathbf{E}_z^p + \frac{\Delta\sigma_i A}{12}$$

$$+ \begin{pmatrix} 2\mathbf{E}_{y1}^p + \mathbf{E}_{y2}^p + \mathbf{E}_{y3}^p \\ \mathbf{E}_{y1}^p + 2\mathbf{E}_{y2}^p + \mathbf{E}_{y3}^p \\ \mathbf{E}_{y1}^p + \mathbf{E}_{y2}^p + 2\mathbf{E}_{y3}^p \end{pmatrix} \tag{18}$$

To find $\frac{\partial \mathbf{h}}{\partial \sigma_i}$, we derive the equations (17) and (18) and obtain:

$$\frac{\partial \mathbf{F}_{tm}}{\partial \sigma_i} = -\frac{\hat{z} c_i}{6u^2} \sum \mathbf{E}_x^p \left(1 - \frac{\Delta\hat{y} i\omega\mu_0}{u^2}\right)$$

$$+ \frac{\hat{z} b_i}{6u^2} \sum \mathbf{E}_z^p \left(1 - \frac{\Delta\hat{y} i\omega\mu_0}{u^2}\right). \tag{19}$$

$$\frac{\partial \mathbf{F}_{te}}{\partial \sigma_i} = -\frac{ik_y b_i}{6u^2} \sum \mathbf{E}_x^p \left(1 - \frac{\Delta\hat{y} i\omega\mu_0}{u^2}\right)$$

$$-\frac{ik_y c_i}{6u^2} \sum \mathbf{E}_z^p \left(1 - \frac{\Delta\hat{y} i\omega\mu_0}{u^2}\right) + \frac{A}{12} \begin{pmatrix} 2\mathbf{E}_{y1}^p + \mathbf{E}_{y2}^p + \mathbf{E}_{y3}^p \\ \mathbf{E}_{y1}^p + 2\mathbf{E}_{y2}^p + \mathbf{E}_{y3}^p \\ \mathbf{E}_{y1}^p + \mathbf{E}_{y2}^p + 2\mathbf{E}_{y3}^p \end{pmatrix}. \tag{20}$$

From the terms $\frac{\partial \mathbf{h}}{\partial \sigma_i}$ and $\frac{\partial \mathbf{S}}{\partial \sigma_i}\mathbf{x}$, we can solve the system found in the equation (10), since the matrix is already in the factored form, remaining to make the backsubstitution using the Gaussian Elimination method.

Perturbation Method (Brute Force)

In order to validate the application of the self-adjoint method for calculating the jacobian matrix associated with MCSEM, we used the Perturbation Method (Brute Force) as a comparison for calculating the numerical derivative. This methodology is the calculation of the derivative using finite difference of first order in which we calculate the functional in relation to the parameter displaced by a delta quantity.

$$\frac{\partial \mathbf{E}_x^s}{\partial \sigma_i} \approx \frac{\Delta \mathbf{E}_x^s}{\Delta \sigma_i} = \frac{\mathbf{E}_x^s(\sigma_i + \delta_\sigma) - \mathbf{E}_x^s(\sigma_i - \delta_\sigma)}{2\delta_{\sigma_i}}. \tag{21}$$

This result is used in the equations (4) and (5) to calculate the derivative of the natural logarithm of the amplitude and the phase of the field $\mathbf{E}_x^s$ in order to compose the jacobian matrix.

Results and Discussions

Now, we will approach the validation of the self-adjoint method by comparing with data obtained by the perturbation method using the modeling done in the code developed by Silva (2012).

The comparison was made using a model that corresponds to the stratified environment composed of air, sea and sediment with resistivities equal to $10^{12}\Omega$ .m, 0.3 Ω .me 1 Ω .m, respectively . The thickness of the sea is 1 km and the sedimentary layer corresponds to the substrate, where the inversion grid is located with 12 parameters arranged from -3 km to 3 km in x and 1100 m to 2100 m in z, with all parameters equal to 100 Ω .m. In this comparison, we used a single frequency equal to 0.5 Hz. The transmitter was positioned at the origin at x, at a depth of 950m, therefore, within the marine layer. The position of the observations were distributed from -15 km to 15 km in the x direction, spaced 200 m from each other on the ocean floor (1 km).

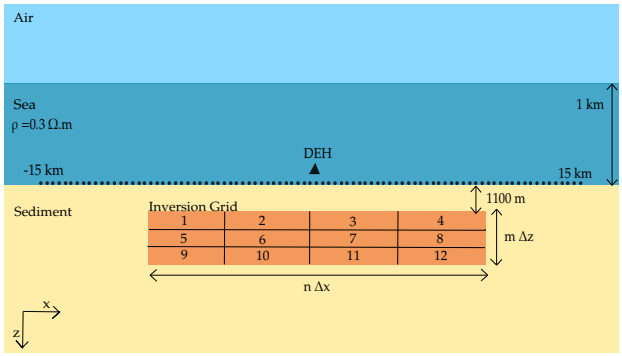

Figure 1: 2D geoelectric model that represents the geological environment of the problem.

In finite element modeling, we use the mesh with dimensions of -55 km to 55 km in the x direction and -40 km to 35 km in the z direction ensuring the homogeneous Dirichlet boundary conditions for the secondary fields. It was made using the Triangle software, which generates unstructured meshes. The figure 2 shows the mesh used in this work, which has 17,140 nodes and 34,147 elements. In the figure 3, we show in more detail the discretization of the inversion grid and the measurement positions of the calculated field.

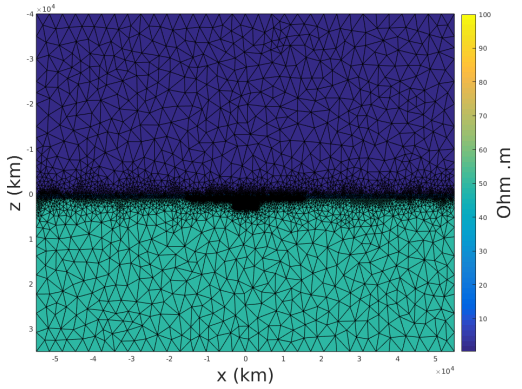

Figure 2: Geoelectric model mesh associated with the marine controlled source method.

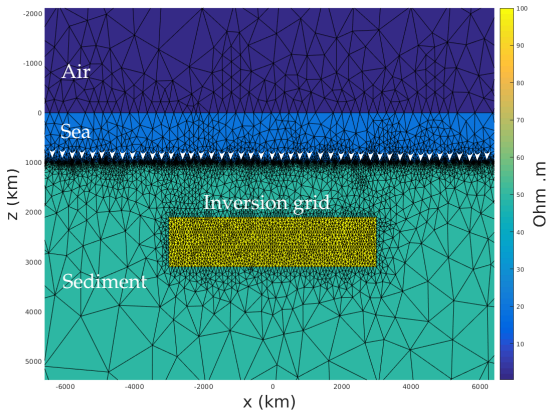

Figure 3: Zoom in the region of inversion in the mesh of the geoelectric model associated with the marine controlled source method.

In this work, we are simulating the acquisition of the inline component of the MCSEM method and calculating the derivatives of these observations in relation to the parameters. The result of the direct problem is shown in the figure 4, in response to the model described above. We emphasize that the secondary component presented is the result of the mathematical formulation of finite elements for the solution of the problem, in which we separate the total field into primary and secondary components, the latter being calculated according to the equation 1.

The graphs bellow show the amplitude (figure 4-a) and phase (figure 4-b) of the total and secondary field in relation to the offset, respectively. In these results, we observe the symmetry of the responses in relation to the position of the transmitter, we also observe the field decreasing with the increase of the offset and greater variations of this decay occur at points around 2 km and 7 km, in the total field, for both positive and negative offset values. These variations are associated with the direct wave (2km) and the air wave (10km).

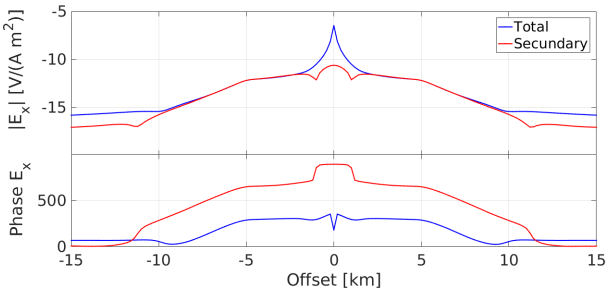

Figure 4: Log10 of the amplitude of the inline component (top) and phase (bottom) for the model with a frequency of 0.50 Hz.

The figure 5 shows the results of the jacobian matrix related to parameters 1 and 4, located in symmetrical positions in relation to the source at the same level as the inversion grid. Analyzing the answers, the great agreement between the two methods used is evident. We also observed the perfect symmetry between the responses of the two parameters, which corroborates the implementation of the Self-Adjoint State method.

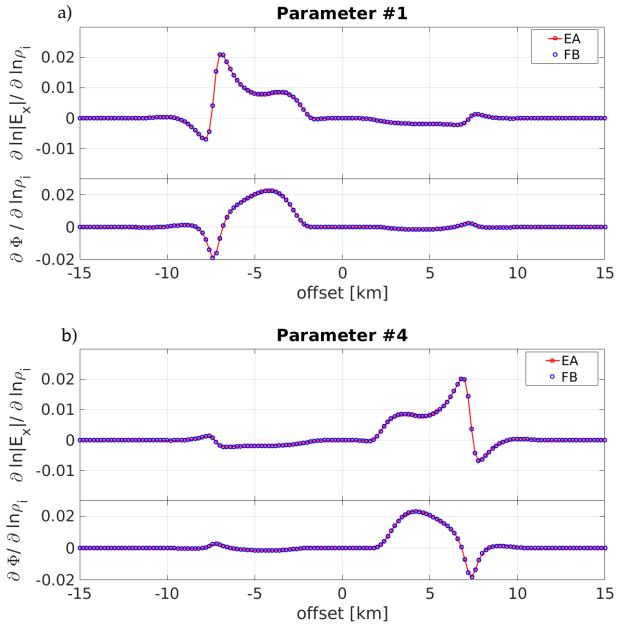

Figure 5: Jacobian matrix columns calculated using Brute Force (FB) and adjoint-state method (EA) for parameter 1 (a) separated in amplitude (top) and phase (bottom) and for parameter 4 (b) separated in amplitude (top) and phase (bottom).

In figure 6, we can observe, in the amplitude graphs, maximum variation due to the change in the parameter around the 5 km offset, while the high derivative value close to 7 km occurs due to the effect of the air wave in this region. In the phase, the effect of the air wave appears in negative values around 7km, with the variation by the perturbation in the parameter being highlighted in the positive part. It is important to note the presence of a peak around x = 7 km, which occurs by changing the parameter, as cells 9 and 12 are located from -3km to -1.5 km and 1.5 km to 3 km in x, respectively. So, there is still a small influence on the opposite side of the offset. From figures 5 and 6, we can see the variation in amplitude derivate and on the phase. This smaller amplitude is due to the greater depth of parameters 9 and 12, however the maximum ones, due to the transition zone for the wave, remain practically constant.

In figure 7, we can see that the effect of the parameter variation on the amplitude and phase derivative occurs in practically the same region as the outermost parameters seen above. This is because at offsets from -2 to 2 km we have the direct wave region, which is not sensitive to variations in sediment properties. However, the anomalies of parameters 10 and 11, in general, have smaller amplitudes than those of parameters 9 and 12.
We will show the percentage absolute error for the calculation of the jacobian using the brute force and Self-Adjunct State given by the equations 4 and 5.

In the graphs of figure 8, the percentage absolute error for parameters 1 and 4 separated into amplitude and phase are presented. It is possible to see in all graphs the highest error values, approximately -2 for amplitude and -6 for phase, occurring in the area of influence of the parameter

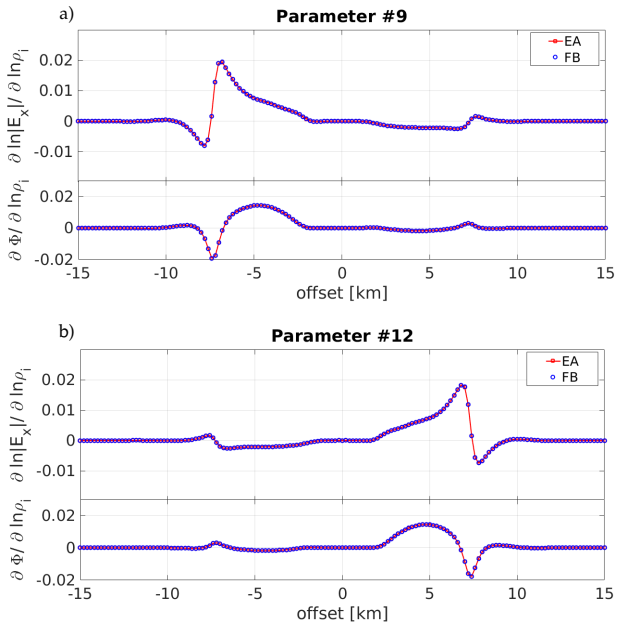

Figure 6: Jacobian matrix columns calculated using Brute Force (FB) and adjoint-state method (EA) for parameter 9 (a) separated in amplitude (top) and phase (bottom) and for parameter 12 (b) separated in amplitude (top) and phase (bottom)

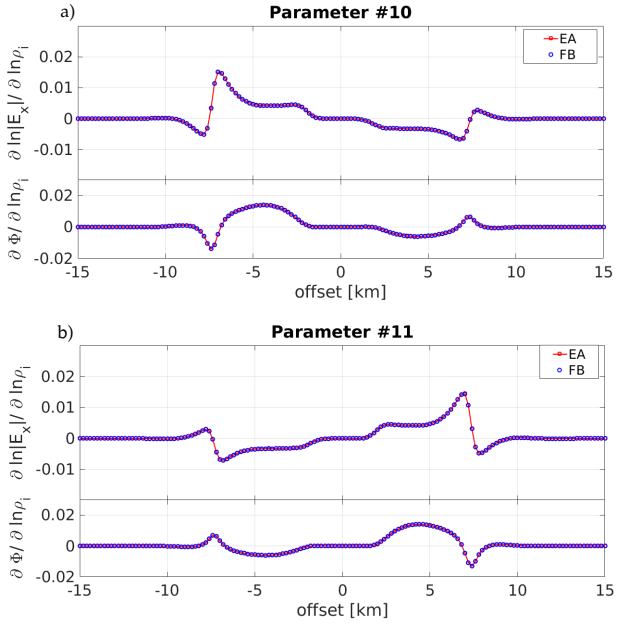

Figure 7: Jacobian matrix columns calculated using Brute Force (FB) and adjoint-state method (EA) for parameter 10 (a) separated in amplitude (top) and phase (bottom) and for parameter 11 (b) separated in amplitude (top) and phase (bottom).

disturbance.

The absolute errors for parameters 9 and 12 are shown in figure 9, in which the error decrease is noticeable in relation to the graphics in figure 8. However, there is still a variable error from -10 to -2 in the amplitudes and from -10 to -6

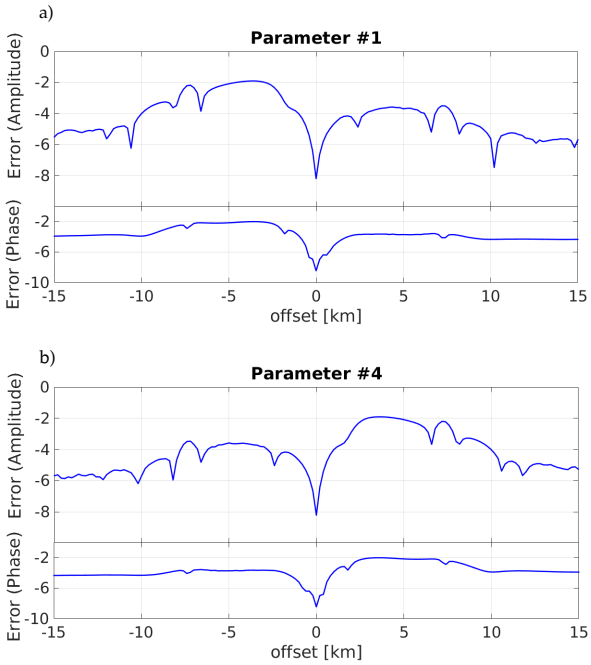

Figure 8: Absolute percentage error in log_{10} between the columns of the jacobian matrix calculated using brute force (FB) and Self-Adjunct State (EA) for parameter 1 (a) in amplitude (top) and phase (bottom); and for parameter 4 (b) in amplitude (top) and phase (bottom).

phases in the region of influence of the parameter.

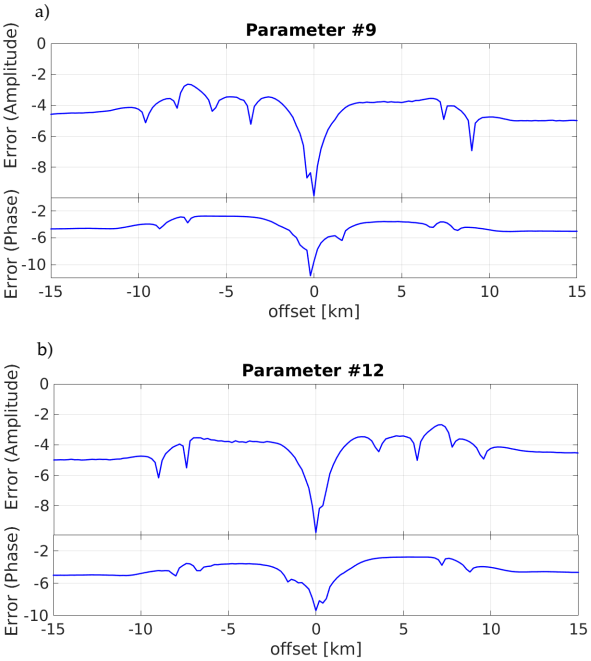

Figure 9: Absolute percentage error in log_{10} between the columns of the jacobian matrix calculated using brute force (FB) and Self-Adjunct State (EA) for parameter 9 (a) in amplitude (top) and phase (bottom); and for parameter 12 (b) in amplitude (top) and phase (bottom).

The time used to run the model 1 problem was 1 hour and

20 minutes for the Brute Force and 9.2 minutes for the Self-Adjunct State, approximately. The experiments were carried out on a machine with an Intel Core i7 processor at 1.80 GHz with 4 cores.

Conclusions

The application of the self-adjoint method proved to be an excellent option for the calculation of the jacobian matrix for the MCSEM 2.5D.

Through the tests performed, we showed that the presented implementation is quite robust when compared with the responses of the perturbation method, both in relation to the symmetry of the responses and the values of the amplitude and phase derivative of the inline component of the electric field.

In a next work step, the algorithms implemented here will be able to integrate an mCSEM 2D data inversion routine.

Acknowledgments

Acknowledgments to the Faculty of Geophysics at UFPA for supporting the development of this work and for the support given to the research scholarship of the project Studies of Electromagnetic Methods Applied to the Exploration of Hydrocarbons, a cooperation term between Petrobras/UFPa/Fadesp .

References

Bakr, S. A., and T. Mannseth, 2009, Feasibility of simplified integral equation modeling of low-frequency marine csem with a resistive target: Geophysics, **74**, F107–F117.

Bakr, S. A., and D. Pardo, 2014, A secondary field based fourier finite element method for the simulation of 3d marine csem measurements, *in* SEG Technical Program Expanded Abstracts 2014: Society of Exploration Geophysicists, 669–673.

Buonora, M. P. P., J. L. Correa, L. S. Martins, P. T. Menezes, E. J. Pinho, J. L. Silva Crepaldi, M. P. Ribas, S. M. Ferreira, and R. C. Freitas, 2014, mcsem data interpretation for hydrocarbon exploration: A fast interpretation workflow for drilling decision: Interpretation, **2**, SH1–SH11.

Constable, S. C., R. L. Parker, and C. G. Constable, 1987, Occam's inversion: A practical algorithm for generating smooth models from electromagnetic sounding data: Geophysics, **52**, 289–300.

Frenkel, M., and S. Davydycheva, 2009, A modeling study of low-frequency csem in shallow water: 71st EAGE Conference and Exhibition incorporating SPE EUROPEC 2009, European Association of Geoscientists & Engineers, cp–127.

Gomes, K. P., and M. W. C. Silva, 2021, Efficient calculation of the jacobian matrix for 3d inversion of mt dat.

Gribenko, A., and M. Zhdanov, 2007, Rigorous 3d inversion of marine csem data based on the integral equation method: Geophysics, **72**, WA73–WA84.

Li, G., and Y. Li, 2017, Joint inversion for transmitter navigation and seafloor resistivity for frequency-domain marine csem data: Journal of Applied Geophysics, **136**, 178–189.

Li, G., Y. Li, and Y. Liu, 2013, Marine csem inversion using the qn-bfgs method: Near Surface Geophysics Asia Pacific Conference, Beijing, China 17-19 July 2013, Society of Exploration Geophysicists, Australian Society of Exploration . . . , 645–649.

Maaø, F. A., 2007, Fast finite-difference time-domain modeling for marine-subsurface electromagnetic problems: Geophysics, **72**, A19–A23.

Moghadas, D., M. Engels, and K. Schwalenberg, 2015, 1d joint multi-offset inversion of time-domain marine controlled source electromagnetic data: Geophysical Prospecting, **63**, 1334–1354.

Nalepa, M., S. Ansari, and C. Farquharson, 2016, Finite-element simulation of 3d csem data on unstructured meshes: An example from the east coast of canada, *in* SEG Technical Program Expanded Abstracts 2016: Society of Exploration Geophysicists, 1048–1052.

Nguyen, A. K., J. I. Nordskag, T. Wiik, A. K. Bjørke, L. Boman, O. M. Pedersen, J. Ribaudo, and R. Mittet, 2016, Comparing large-scale 3d gauss–newton and bfgs csem inversions, *in* SEG Technical Program Expanded Abstracts 2016: Society of Exploration Geophysicists, 872–877.

Peng, R., and X. Hu, 2015, 3d inversion of marine controlled-source electromagnetic data using an inexact gauss newton method, *in* SEG Technical Program Expanded Abstracts 2015: Society of Exploration Geophysicists, 1001–1005.

Ramananjaona, C., L. MacGregor, and D. Andréis, 2011, Sensitivity and inversion of marine electromagnetic data in a vertically anisotropic stratified earth: Geophysical Prospecting, **59**, 341–360.

Rijo, L., W. Pelton, E. Feitosa, and S. Ward, 1977, Interpretation of apparent resistivity data from apodi valley, rio grande do norte, brazil: Geophysics, **42**, 811–822.

Shragge, J., T. Yang, and P. Sava, 2013, Time-lapse image-domain tomography using adjoint-state methods: Geophysics, **78**, A29–A33.

Silva, H. F., 2012, Modelagem numérica de dados mcsem 2.5-d: Dissertação de mestrado, Universidade Federal do Pará - CPGF, Belém-PA.

Taillandier, C., M. Noble, H. Chauris, and H. Calandra, 2009, First-arrival traveltime tomography based on the adjoint-state method: Geophysics, **74**, WCB1–WCB10.

Tarantola, A., and B. Valette, 1982, Generalized nonlinear inverse problems solved using the least squares criterion: Reviews of Geophysics, **20**, 219–232.

Ueda, T., and M. S. Zhdanov, 2005, Fast numerical modeling of marine controlled-source electromagnetic data using quasi-linear approx-imation, *in* SEG Technical Program Expanded Abstracts 2005: Society of Exploration Geophysicists, 506–509.

Zach, J. J., M. A. Frenkel, et al., 2012, 3d inversion-based interpretation of marine csem data: SPE Reservoir Evaluation & Engineering, **15**, 321–334.